



In the format provided by the authors and unedited.

Effects of primitive photosynthesis on Earth's early climate system

Kazumi Ozaki ^{1,2,3*}, Eiichi Tajika ⁴, Peng K. Hong⁵, Yusuke Nakagawa⁶ and Christopher T. Reinhard^{1,2}

¹School of Earth and Atmospheric Sciences, Georgia Institute of Technology, Atlanta, GA, USA. ²NASA Astrobiology Institute, Alternative Earths Team, Mountain View, CA, USA. ³NASA Postdoctoral Program, Universities Space Research Association, Columbia, MD, USA. ⁴Department of Earth and Planetary Science, Graduate School of Science, The University of Tokyo, Bunkyo-ku, Tokyo, Japan. ⁵Department of Systems Innovation, School of Engineering, The University of Tokyo, Bunkyo-ku, Tokyo, Japan. ⁶Analysis Engineering Department, Hitachi Power Solutions Co., Ltd., Hitachi-Shi, Ibaraki, Japan. *e-mail: kazumi.ozaki@eas.gatech.edu

Supplementary Information for

Effects of primitive photosynthesis on Earth's early climate system

Kazumi Ozaki^{*}, Eiichi Tajika, Peng K. Hong, Yusuke Nakagawa, and Christopher T. Reinhard

^{*}Corresponding author. E-mail: kazumi.ozaki@eas.gatech.edu

1 Supplementary Methods

Mechanistic framework. The central aim here is to provide a quantitative framework of global redox balance model for evaluating the biogenic CH₄ cycle in the Archaean anoxic world, with particular emphasis on the critical role of photoferrotrophs in the redox balance. This exercise not only helps to elaborate on the theoretical underpinning of the results from the coupled model presented in the main text but also facilitates exploration of wide range of parameter space at reduced calculation cost with reasonable quantitative accuracy.

The system considered in this study is shown in Figure 1 of the main text. The primary source of reducing power (in terms of H₂) is outgassing of reduced gases from the Earth's interior. The sink fluxes are an irreversible escape of hydrogen to space and deposition of organic matter to the sediments. For our purposes we concern ourselves only with times prior to the advent of

oxygenic photosynthesis. Because anoxygenic phototrophy was probably a dominant mode of primary productivity by the early Archaean, we consider an ecosystem driven by anoxygenic phototrophic organisms. Despite the fact that the lateral transfer of genetic material has affected microbial genomes, the assumption that anoxygenic phototrophic bacteria evolved before oxygen-producing cyanobacteria is generally accepted because it appears to require the earlier evolution of at least two types of photosystems (i.e., photosystems I and II). The simple microbial ecosystem considered here includes two primary producers (i.e., H₂-using (R1) and Fe²⁺-using anoxygenic phototrophs (R5)) and secondary organisms (i.e., Fe(III) reducers (R6), fermentors (R3) and methanogens (R4)). CO-based chemotrophy (R2) is, for now, not included, but its inclusion should not significantly alter our results (see the model description of the coupled model which explicitly takes into account CO-based chemotrophs). The biological metabolisms included in this study are summarized in Supplementary Table 1. In this study, we focus primarily on the critical synergistic effect of H₂-based and Fe²⁺-based photosynthesis on the global CH₄ cycle and do not elaborate on the role of H₂-using methanogens as a primary producer because they basically show similar behaviour to that of H₂-based anoxygenic photosynthesis^{1,2} (see Supplementary Discussion for the representative results). The following exercise is based mainly on the analytical approach of ref.¹, and the modifications and assumptions are summarized below.

Under almost completely anoxic conditions (atmospheric O₂ levels <10⁻⁵ present atmospheric level; PAL), hydrogen vented from the Earth's interior can accumulate to substantial levels in the atmosphere. Previous studies^{1,2} have argued that anoxygenic photosynthesis with hydrogen

would have been one of the most active ecosystems at that time. The metabolic reaction is written as:



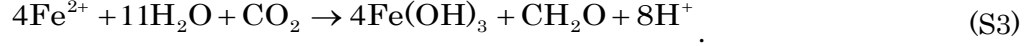
We assume, as in ref.¹, that H₂-using anoxygenic phototrophs can utilize all H₂ entering the ocean from the atmosphere. In other words, the primary production of H₂-using photosynthesis, flux_{marH₂} (in unit of molecules H₂ cm⁻² s⁻¹), is limited by the flux of H₂ across the air-sea interface, and the concentration of hydrogen in the surface ocean is assumed to be 0. The upwelling delivery of H₂ was ignored here because it plays a minor role when atmospheric *p*H₂ is larger than ~10 ppmv, even if the extreme value of 100 nM is assumed³. The downward flux of H₂ across the air-sea interface is evaluated using the stagnant boundary layer model (see below), giving rise to the following expression for flux_{marH₂}:

$$\text{flux}_{\text{marH}_2} = v_p D \alpha p\text{H}_2 \quad (\text{S2})$$

where *v_p* is a piston velocity of H₂ (0.013 cm s⁻¹), *D* is a constant of proportionality for converting to the flux units used here (6.02×10²⁰ molecules cm⁻³ mol⁻¹ l), *α* represents the Henry's law coefficient for H₂ (7.8×10⁻⁴ M atm⁻¹), and *p*H₂ is the mixing ratio of hydrogen just above the surface ocean. From equation (S1), 2 mole of hydrogen is used to produce 1 mole of organic matter, and therefore, primary production of organic carbon by H₂-using anoxygenic photosynthesis, *NPP*_{H₂-photo}, can be represented by flux_{marH₂}/2.

It is thought that the early Archaean oceans were essentially under anoxic, and probably ferruginous (i.e., anoxic and Fe²⁺-rich) conditions⁴. Under such conditions, Fe²⁺-using anoxygenic phototrophs (photoferrotrophs) should play a major role in primary production. In

this case Fe^{2+} is utilized as an electron source for carbon fixation and biomass formation. The metabolic stoichiometry is conventionally written as follows:



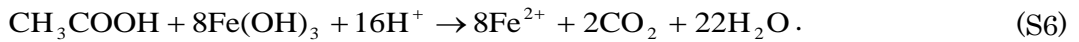
By assuming that the activity of photoferrotrophs is limited by the flux of ferrous iron to the surface ocean, $\text{flux}_{\text{iron}}$, primary production of organic matter by photoferrotrophs can be written as $\text{flux}_{\text{iron}}/4$. The total net primary production, *NPP* (in terms of organic carbon), is therefore given by

$$NPP = \frac{\text{flux}_{\text{marH}_2}}{2} + \frac{\text{flux}_{\text{iron}}}{4} \quad (\text{S4})$$

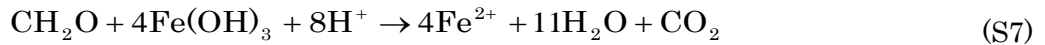
We assume that fermenting microorganisms, which are thought to be very ancient, would have been an important component of the Archaean biosphere. The fermentation of organic matter originating from primary producers yields acetic acid:



The capacity for dissimilatory iron reduction is widely distributed among a number of bacteria and Archaea⁵. If ferric hydroxide, $\text{Fe}(\text{OH})_3$, is available, acetic acid will be converted to CO_2 by microbial dissimilatory Fe(III) reduction:



The net result of fermentation and iron reduction combined is:



The significance of this metabolic pathway in the Archaean oceans remains quite uncertain^{6,7}.

We introduce a free parameter, γ , which represents the fraction of $\text{Fe}(\text{OH})_3$ that is reduced to Fe^{2+}

by dissimilatory Fe(III) reduction (equation (S6)). The burial rate of Fe(OH)₃, $\text{flux}_{\text{bur}}^{\text{Fe(OH)}_3}$, is therefore given by:

$$\text{flux}_{\text{bur}}^{\text{Fe(OH)}_3} = (1 - \gamma) \times \text{flux}_{\text{iron}} \quad (\text{S8})$$

The alternative pathway of decomposition of organic matter takes place via acetotrophic methanogenesis:



In this case, the overall metabolic pathway (equation (S5) + equation (S9)) is



It is important to note that it remains unclear whether acetoclastic methanogens existed on the Archaean Earth. A recent phylogenetic analysis⁸ suggests that acetoclastic *Methanosarcina* did not evolve until the Permian. However, there are species of the other genus of acetoclastic methanogens *Methanosaeta* which likely evolved much earlier than *Methanosarcina*. According to Rothman et al.⁸, the emergence of *Methanosaeta* appears to be ~1700 Ma, but given a poor archaeal root calibration and an intrinsic uncertainty in molecular clock estimates, the exact timing for the ancestor of *Methanosaeta* remains elusive and we consider our assumption that acetoclastic methanogens existed in the Archaean ocean defensible null hypothesis. Also, even if acetoclastic methanogens did not exist in Archaean oceans, we can invoke alternative pathways for methane generation; for example, a symbiotic system between anaerobic oxidation of acetate and H₂-based methanogens. The net stoichiometry is identical to that of acetoclastic methanogens (equation (S9)). In this case, H₂-using methanogens plays a critical role in methane generation (see Supplementary Discussion).

We assume that a certain fraction, x , of the organic matter produced by producers will escape the decomposition processes and bury in sediments:

$$\text{flux}_{\text{bur}}^{\text{CH}_2\text{O}} = x \times NPP, \quad (\text{S11})$$

where $\text{flux}_{\text{bur}}^{\text{CH}_2\text{O}}$ represents the burial rate of organic carbon. We also assumed that CH_4 produced via the above sequence of reactions in the anoxic ocean interior can readily escaped to the atmosphere with limited consumption via anaerobic methane oxidation (AOM) ($\text{CH}_4 + \text{SO}_4^{2-} \rightarrow \text{HS}^- + \text{HCO}_3^- + \text{H}_2\text{O}$). This assumption is based on the notion that the Archaean oceans were strongly deficient in SO_4^{2-} (ref. ^{9, 10}). However, it has been shown that one of the archaeal groups (ANME-2) has an ability to use iron and manganese oxide as electron acceptors instead of sulphate¹¹. In any case, the uncertainty associated with AOM is implicitly accounted for by examining uncertainty in γ , and we emphasize that additional sinks for methane in our model would only further implicate our ‘hybrid’ biosphere are being critical for supporting warm climate states.

Overall, the biogenic CH_4 flux to the atmosphere, $\text{flux}_{\text{methane}}$, is given by

$$\text{flux}_{\text{methane}} = \frac{1}{2} \left\{ (1-x)NPP - \gamma \frac{\text{flux}_{\text{iron}}}{4} \right\}. \quad (\text{S12})$$

As the dissimilatory iron reduction decreases in importance (i.e., $\gamma \rightarrow 0$), methane degassing from the ocean to the atmosphere increases, for given x and NPP . In contrast, a significant role of iron reducers in the remineralization of organic matter suppresses the biogenic methane generation in the ocean interior. Note that there is an upper limit for γ , at which all degradable organic matter is oxidized by Fe(III) reduction (see below).

The atmospheric model of ref.¹² provides a relationship between biogenic methane flux to the atmosphere and the mixing ratio of methane in the atmosphere, $f(\text{CH}_4)$, for the range of 10^{-5} – 10^{-3} . Canfield et al.¹ have proposed a linear relationship on the basis of fitting to the model results presented in ref.¹²:

$$f(\text{CH}_4) = \frac{\text{flux}_{\text{methane}}}{10^{14.43}}, \quad (\text{S13})$$

where $\text{flux}_{\text{methane}}$ has a unit of $\text{cm}^{-2} \text{s}^{-1}$. Although the linear relationship is a crude approximation (it predicts an order of magnitude lower $f(\text{CH}_4)$ than photochemical model when $\text{flux}_{\text{methane}} > 1.5 \times 10^{11} \text{cm}^{-2} \text{s}^{-1}$; Supplementary Fig. 1a), it captures the first-order characteristics of atmospheric model, and more importantly, it enables us to obtain an analytical solution (see below). We therefore apply equation (S13) as a first step, but also explore an alternative fitting function (see Methods).

In an anoxic H_2 -bearing atmosphere, hydrogen escape to space plays a significant role in the global hydrogen balance. If it is diffusion-limited, as it is today, the total concentration of all H-bearing compounds in the lower stratosphere determines the rate of hydrogen escape¹³. For the atmospheres examined in this study, H_2 and CH_4 appear to have been dominant hydrogen-bearing species in the stratosphere, and the flux, flux_{esc} (in unit of $\text{cm}^{-2} \text{s}^{-1}$), is calculated as

$$\text{flux}_{\text{esc}} = A \times [f(\text{H}_2) + 2f(\text{CH}_4)], \quad (\text{S14})$$

where A is an average bimolecular diffusion parameter for H and H_2 in air divided by the atmospheric scale height ($2.5 \times 10^{13} \text{cm}^{-2} \text{s}^{-1}$) and $f(\text{X})$ represents the mixing ratio of the species of X in the stratosphere. It is also assumed that the partial pressures of H_2 and CH_4 in the air just

above the ocean surface are similar to the mixing ratios of these gases in the stratosphere (i.e., $pX = f(X)$)¹ because the vertical profiles of H₂ and CH₄ below the stratosphere are generally well-mixed.

Redox balance exerts a primary control on the chemistry of the ocean-atmosphere system. For example, the source flux of hydrogen to the ocean-atmosphere system is volcanic outgassing, $\text{flux}_{\text{volc}}$, representing an input of reducing power. Based on Kharecha et al.² and Kasting¹⁴, we define “neutral” oxidation states for compounds containing hydrogen, carbon, nitrogen, iron, and sulphur; H₂O, CO₂, N₂, FeO, and SO₂, and reducing power is measured in units scaled to the reducing power of an H₂ molecule that is defined as +1. Then, the reducing power of a series of species, Φ , is determined (Supplementary Table 2). For example, the burial of Fe(OH)₃ is a loss of oxidative power, i.e. an input of reducing power, and burial of organic matter can be regarded as a sink of the reducing power. At steady state, the sum of the source fluxes of reducing power should be balanced by the sink fluxes, i.e., hydrogen escape and burial of organic matter. The redox-balanced equilibrium of the system is given by

$$\Phi_{\text{H}_2} \text{flux}_{\text{volc}} + \Phi_{\text{Fe(OH)}_3} \text{flux}_{\text{bur}}^{\text{Fe(OH)}_3} = \Phi_{\text{H}_2} \text{flux}_{\text{esc}} + \Phi_{\text{CH}_2\text{O}} \text{flux}_{\text{bur}}^{\text{CH}_2\text{O}} \quad (\text{S15})$$

Plugging equations (S4), (S8) and (S11) into equation (S15) leads us to a following relationship:

$$\text{flux}_{\text{volc}} + \frac{1}{2}(1-\gamma)\text{flux}_{\text{iron}} = \text{flux}_{\text{esc}} + 2x \left(\frac{\text{flux}_{\text{marH}_2}}{2} + \frac{\text{flux}_{\text{iron}}}{4} \right). \quad (\text{S16})$$

With above equations and assumptions, we can obtain an analytical solution at steady state. By combining equations (S2), (S4), (S12)–(S14), the following relation is obtained:

$$\text{flux}_{\text{volc}} = \left(\frac{A}{V_p \alpha D} + x \right) \text{flux}_{\text{marH}_2} + 4AB \left\{ (1-x) \left(\frac{\text{flux}_{\text{marH}_2}}{2} + \frac{\text{flux}_{\text{iron}}}{4} \right) - \gamma \frac{\text{flux}_{\text{iron}}}{4} \right\} - (1-x-\gamma) \frac{\text{flux}_{\text{iron}}}{2},$$

where B is a constant ($1/(4 \times 10^{14.43}) = 9 \times 10^{-16}$ molecules⁻¹ cm² s⁻¹). By solving this with respect to $\text{flux}_{\text{marH}_2}$, we obtain equation (1) in Methods.

Note that we assume that ferric oxyhydroxides represent the ultimate phase of iron removal from the system. If the deposited iron was converted to other phases, such as magnetite, during diagenesis or metamorphism, the impact of iron removal on the redox balance is slightly altered¹⁴ (the formation of magnetite yields slightly less hydrogen; 1/3 mol of H₂ per mole of Fe). We neglect this here for simplicity.

It is also important to note that there is an upper limit on γ , at which all degradable organic matter is oxidized by Fe(III) reduction. By setting equation (S12) at zero and combining equation (S4), the following relationship is obtained:

$$\gamma_{\text{max}} = (1-x) \left(1 + 2 \frac{\text{flux}_{\text{marH}_2}}{\text{flux}_{\text{iron}}} \right). \quad (\text{S17})$$

When $\gamma = \gamma_{\text{max}}$, there is no biogenic methane flux, meaning atmospheric $p\text{CH}_4 = 0$. Then, hydrogen balance in the atmosphere can be written as follows:

$$\text{flux}_{\text{volc}} = \text{flux}_{\text{marH}_2} + \text{flux}_{\text{esc}}. \quad (\text{S18})$$

By substituting equations (S2) and (S14), this equation can be solved with respect to $\text{flux}_{\text{marH}_2}$:

$$\text{flux}_{\text{marH}_2} = \text{flux}_{\text{volc}} \left(1 + \frac{A}{V_p \alpha D} \right)^{-1}. \quad (\text{S19})$$

Therefore, γ_{\max} can be written in terms of model parameters, as follows;

$$\gamma_{\max} = (1 - x) \left\{ 1 + 2 \left(1 + \frac{A}{V_p \alpha D} \right)^{-1} \frac{\text{flux}_{\text{volc}}}{\text{flux}_{\text{iron}}} \right\}. \quad (\text{S20})$$

A coupled atmosphere-ocean ecosystem model. The photochemical model used in this study is a one-dimensional model originally developed by Pavlov et al¹². The model includes 73 chemical species (39 long-lived species, 31 short-lived species, and 3 aerosols particles) (Supplementary Table 3) involved in 359 chemical reactions. The model includes transport by eddy and molecular diffusion over a 100 km with 1 km grid spacing. The governing equation is given by

$$N \frac{\partial f_i}{\partial t} = P_i - L_i N f_i - \frac{\partial \Phi_i}{\partial z}, \quad (\text{S21})$$

where N (in cm^{-3}) is the number density of molecules in air, f_i is the mixing ratio of molecular species i , and the combined first and second term on the right hand side ($P_i - L_i N f_i$) (in $\text{cm}^{-3} \text{s}^{-1}$) is a net production rate of molecular species i . The vertical transport efficiency is expressed as Φ_i (in $\text{cm}^{-2} \text{s}^{-1}$), which includes the effects of both molecular and eddy diffusion:

$$\Phi_i = D_i N \left(\frac{1}{H_a} - \frac{1}{H_i} \right) - (D_i - K) N \frac{\partial f_i}{\partial z}, \quad (\text{S22})$$

where D_i (in $\text{cm} \text{s}^{-1}$) denotes the molecular diffusion coefficient of molecular species i ;

$$D_i = 1.52 \times 10^{18} \times \sqrt{\left(\frac{1}{M_i} - \frac{1}{M} \right) \frac{\sqrt{T(z)}}{n_a(z)}}. \quad (\text{S23})$$

M_i is a molecular weight of species i , M is molecular weight of atmosphere, $T(z)$ (in K) is temperature at altitude z , and $n_a(z)$ is a number density of air (in cm^{-3}). Vertical profiles of temperature and number density assumed in the model are shown in Supplementary Fig. 2a,b.

For an eddy diffusion profile, we adopted the observational result on present Earth¹⁵ (Supplementary Fig. 2c).

The model simulates an anoxic 1 bar atmosphere and variable amounts of H, C, N, and S species. The solar zenith angle was set at 50°. The continuity equation was solved at each height for each of the long-lived species, including transport by eddy and molecular diffusion. The combined equations were cast in centered finite difference form. Boundary conditions were set for each species at the top and bottom of the atmosphere, and the resulting set of coupled differential equations was integrated to steady state using the reverse Euler method. A two-stream approach was used for radiative transfer. We did not perform coupled climate model calculations; rather, we simply assumed that the temperature decreases with height from 298 K at the surface to 180 at 12.5 km, following a moist adiabat. Above that height, the atmosphere was assumed to be isothermal (Supplementary Fig. 2a). Volcanic outgassing of H₂ and other reduced species was included. The volcanic H₂ input flux was treated as one of the sensitivity parameters. No abiotic source of methane is included in this study. The mixing ratio of NH₃ is fixed to 1×10⁻¹⁰. The volcanic outgassing rate of SO₂ and H₂S was set at 3.8×10⁸ cm⁻² s⁻¹.

To evaluate the gas exchange flux at the air-water interface, we adopted the stagnant boundary layer model, following Kharecha et al.². The flux of gas X across the air-water interface is evaluated as the product of its piston velocity (v_p) and its concentration gradient between the top and the bottom of the boundary layer ($[X]_{aq}$);

$$\text{flux}_{\text{exchange}}(X) = v_p(X) \times (\alpha(X)pX - [X]_{aq}) \times D, \quad (\text{S24})$$

where α is the Henry's law coefficient, pX is the partial pressure of X in the atmosphere, and C ($= 6.02 \times 10^{20}$ molecules cm^{-3} mol^{-1} L) is a unit conversion factor.

The primary difference between our coupled ocean ecosystem model and the sGRB model is the explicit inclusion of CO-consuming acetogens. We assume, following Kharecha et al.², that CO deposited to the ocean is readily consumed by CO-consuming acetogens ($[\text{CO}]_{\text{aq}} = 0$):



By combining with equation (S9), the overall reaction is given by:



As a result, the biogenic CH_4 flux from the ocean to the atmosphere is modified as follows:

$$\text{flux}_{\text{methane}} = \frac{1}{2} \left\{ (1-x)NPP - \gamma \frac{\text{flux}_{\text{iron}}}{4} \right\} + \frac{1}{4} \text{flux}_{\text{CO}}, \quad (\text{S27})$$

where flux_{CO} is the CO deposition flux from the atmosphere to the ocean and NPP is given by equation (S4). We force $\text{flux}_{\text{methane}}$ as a bottom boundary condition for the photochemical model.

Redox states of the atmosphere, the ocean, and the ocean-atmosphere system should be balanced on the timescale considered here. Based on Kharecha et al.² and Kasting¹⁴, redox balance in the model is tracked in units scaled to the reducing power of H_2 (see above). The photochemistry model explicitly accounts for fluxes of oxidants and reductants into and out of the atmosphere, and redox balance is automatically achieved:

$$F_{\text{volc}} + F_{\text{rain}} + F_{\text{exchange}} + F_{\text{esc}} = 0, \quad (\text{S28})$$

where

$$F_{\text{volc}} = \sum_X \Phi_X \times \text{flux}_{\text{volc},X} , \quad (\text{S29})$$

$$F_{\text{rain}} = \sum_X \Phi_X \times \text{flux}_{\text{rain},X} , \quad (\text{S30})$$

$$F_{\text{exchange}} = F_{\text{flow}} - F_{\text{dep}} = \sum_X \Phi_X \times \text{flux}_{\text{flow},X} - \sum_X \Phi_{\text{dep}} \times \text{flux}_{\text{dep},X} , \quad (\text{S31})$$

$$F_{\text{esc}} = \sum_X \Phi_X \times \text{flux}_{\text{esc},X} . \quad (\text{S32})$$

Here, Φ_X is reducing power of species X (Supplementary Table 2), $\text{flux}_{\text{volc}}$ is the volcanic outgassing flux, $\text{flux}_{\text{rain}}$ is the flux of rainout rate, $\text{flux}_{\text{exchange}}$ is the flux of air-sea gas exchange, flux_{esc} is the rate of escape of reductants out the top of the atmosphere to space. The coupled model also automatically ensures that the redox balance of the ocean-atmosphere system (equation (S15)) is satisfied, for a given set of boundary conditions. In this study we track the redox budget for each simulation, and once redox imbalance in the atmosphere, the ocean, and the ocean-atmosphere system reaches sufficiently small (0.01%) value, the calculation is considered converged.

2 Supplementary Discussion

Role of CO-based chemotrophs. Figure 2 in the main text shows that net primary production of H_2 -using anoxygenic photosynthesis increases with increasing outgassing flux of reduced gases, $\text{flux}_{\text{volc}}$. This can be attributed to an increase in atmospheric H_2 mixing ratio (Supplementary Fig. 4b). We also find that as biological CH_4 degassing from the ocean to the atmosphere increases, the activity of CO-consuming acetogens increases, as evidenced by increasing the mixing ratio of CO in the atmosphere (Supplementary Fig. 4c). The photochemical source of CO is primarily controlled by the photolysis of CO_2 : $\text{CO}_2 + h\nu (\lambda < 175 \text{ nm}) \rightarrow \text{CO} + \text{O}$. CO is also generated

via CH₄ oxidation by hydroxyl radical (OH) ($\text{CH}_4 + \text{OH} \rightarrow \dots \rightarrow \text{CO} + \dots$). CO is oxidized by OH and produce CO₂ as by product ($\text{CO} + \text{OH} \rightarrow \text{CO}_2 + \text{H}$). OH is produced mainly by H₂O photolysis ($\text{H}_2\text{O} + h\nu \rightarrow \text{H} + \text{OH}$), but its absorption spectrum overlaps with those of CH₄ at extreme ultraviolet wavelengths ($\lambda < 140$ nm). Consequently, as flux_{volc} increases, a concomitant increase in CH₄ (Supplementary Fig. 4a) results in an increase in CO level, promoting the activity of CO-consuming acetogens.

Possible errors of the sGRB model. In the sGRB model, an empirical fitting function (equation (2) in Methods) is adopted to assess the atmospheric CH₄ mixing ratio as a function of CH₄ flux to the atmosphere (flux_{methane}). The equation (2) is obtained based on the photochemical model experiments in which atmospheric CO₂ was set at 0.01 bar. It is, however, important to note that the relationship between CH₄ mixing ratio and flux_{methane} is also a function of atmospheric CO₂ levels – lower CO₂ levels lead to lower CH₄ mixing ratio for a given value of flux_{methane}, and vice versa (Supplementary Fig. 1b). However, we do not expect the inclusion of this CO₂ dependency to alter our overarching conclusions. When we set log(*p*CO₂) at -2.3 (~0.005 bar), the sGRB model overestimates the surface temperature by ~3 K. However, warm climate states (≥ 288 K) with CH₄/CO₂ ratio of ≤ 0.2 are not achievable even under such conditions (Fig. 3c,d). In other words, the degree of overestimation by the sGRB model should not be larger than 3 K (and is likely much lower). When the CO₂ mixing ratio is larger than 0.01 bar, our model should be regarded as conservative for the search of warm climate states. Supplementary Figure 5 shows global surface temperature as a function of outgassing rate of reduced gases for different *p*CO₂ values. The sGRB model shows good agreement with the coupled model for *p*CO₂ = 0.01 bar

(Supplementary Fig. 5a) and slightly underestimates surface temperature at higher $p\text{CO}_2$ values (Supplementary Fig. 5b,c).

Evaluating uncertainty in the effect of Fe(III) reduction. It is important to investigate the biogeochemical and climatological effects of dissimilatory iron reduction because we expect that the warming effect by photoferrotrophy tends to be attenuated if Fe(III) reduction plays a dominant role in the organic matter decomposition. However, the quantitative importance of Fe(III) reduction in the Archaean oceans remains uncertain. Konhauser et al.⁷ infer that as much as 70% of the biologically formed ferric hydroxide could have been reducing to Fe^{2+} via microbial Fe(III) reduction during deposition of Archaean banded iron formations (BIFs), based on geological data and laboratory results on the rates of iron reactions. This provides some basis for constraining the value of γ . However, it is important to note that it is unlikely that this value can be scaled globally for the Archaean oceans. It is more realistic to expect that heterogeneity would have existed in the relative importance of photoferrotrophy and Fe(III) reducers due to the spatio-temporal variability in phototrophic activity and depositional environment. Further careful consideration is needed to further constrain the value of γ . However, the important point here is that the acceleration of the biogenic CH_4 cycle by photoferrotrophs would exert a crucial influence on the Archaean climate even if Fe(III) reduction is responsible for as much 70% of organic matter decomposition on a globally integrated basis (Supplementary Fig. 6).

Fe-based ecosystem and climate. To explore the behaviour of our idealized Fe-based ecosystem to changes in Fe^{2+} input flux, we performed an additional sensitivity experiment for an Fe-based

ecosystem with the sGRB model, in which H₂-based anoxygenic phototrophs are removed from the Case 2 biosphere. Supplementary Figure 7 shows the response of atmospheric $f(\text{CH}_4)$ and global surface temperature to changes in Fe²⁺ input flux to the photic zone showing that the conditions for warm climate are rather limited for the Fe-based ecosystem (black lines): Fe²⁺ input flux of $>\sim 400 \text{ Tmol Fe yr}^{-1}$ would be needed even when $\gamma = 0$ —a condition that is very unlikely given reasonable constraints on Fe input fluxes to the exogenic system (see Main text). The result obtained from the Case 2 hybrid ecosystem (red lines) also highlights the crucial role of the synergistic effect of multiple coexisting forms of photosynthetic metabolism in the feasibility of warm climate states: the calculated surface temperature is sustained at above 285 K, irrespective of the Fe²⁺ input flux.

Conditions for warm climate states. Supplementary Figure 8–10 shows the critical relationship between model parameters and probability of warm ($\geq 288 \text{ K}$) climate solutions for the Case 1 (H₂-based) biosphere (Supplementary Fig. 8), the Fe-based biosphere (Supplementary Fig. 9), and the Case 2 hybrid biosphere (Supplementary Fig. 10). In Supplementary Figs. 8 and 9, there are wide “dead zones” where no warm solution exists. For example, warm climate states can only be maintained when $p\text{CO}_2$ is $>\sim 70 \text{ PAL}$ for the Case 1 biosphere, even when we assume a total outgassing rate of reduced gases ($\text{flux}_{\text{volc}}$) equivalent to $10\times$ the present value of $2.9 \text{ Tmol H}_2 \text{ equivalents yr}^{-1}$ (ref.¹⁶). A photosynthetic biosphere based solely on photoferrotrophy (Fe²⁺-using anoxygenic photosynthesis) also requires $p\text{CO}_2$ of $>\sim 50 \text{ PAL}$ and $\text{flux}_{\text{iron}}$ of $>\sim 50 \text{ Tmol Fe yr}^{-1}$, respectively. In contrast, the hybrid biosphere readily expands the region of parameter space that favours stable warm climate states (Supplementary Fig. 10). Specifically, much of the parameter space in Supplementary Fig. 10b,c,d has the potential for warm climate

states as long as $p\text{CO}_2$ is sufficiently high ($>\sim 50$ PAL) (Supplementary Fig. 10a). One of the striking features is that there is a feasible range of the value of $\text{flux}_{\text{iron}}$, where the CO_2 levels required would reach a minimum (Supplementary Fig. 10a). Supplementary Figure 10d also demonstrates that the feasible range of $\text{flux}_{\text{iron}}$ for warm climate is sensitive to the value of γ , as higher γ prevents the acceleration of biogenic CH_4 cycle, larger $\text{flux}_{\text{iron}}$ is required for warm climate as γ increases.

The potential role of H_2 -using methanogens as a primary producer. In this study, we do not discuss the role of H_2 -using methanogens as a primary producer because they basically show similar behaviours to that of H_2 -based anoxygenic photosynthesis^{1, 2}. However, H_2 -based methanogenesis is thought to be an ancient metabolism based on phylogenetic analyses^{17, 18}, and the discovery of isotopically light methane in fluid inclusions from 3.5 Ga cherts from the Pilbara craton in Australia provides geochemical evidence for a very early emergence of methanogenesis¹⁹. Here we explore the potential role of H_2 -using methanogens on the biogenic CH_4 cycling.

The metabolic reaction of H_2 -using methanogens is written as:



The production of organic matter through this reaction is calculated based on the growth yield, y , the ratio of assimilation to metabolism. As in ref.², we assume that these organisms assimilate 1 mole of CO_2 into biomass for every 10 mole they metabolize; i.e., $y = 0.1$. The net primary production is written as:

$$NPP = \frac{y}{2} \text{flux}_{\text{marH}_2}, \quad (\text{S34})$$

where the flux of hydrogen across the sea-water interface is calculated based on equation (S24):

$$\text{flux}_{\text{marH}_2} = v_p \times (\alpha p \text{H}_2 - [\text{H}_2]) \times D. \quad (\text{S35})$$

Methanogens are able to consume dissolved H_2 only until the energy yield is sufficient for ATP production. Canfield et al.¹ adopted 5×10^{-9} M, and we maintain this value here. The biogenic CH_4 flux to the atmosphere is:

$$\text{flux}_{\text{methane}} = \frac{1-x}{2} NPP + \frac{1-y}{4} \text{flux}_{\text{marH}_2}. \quad (\text{S36})$$

The global redox budget is written as:

$$\text{flux}_{\text{volc}} = \text{flux}_{\text{esc}} + 2\text{flux}_{\text{bur}}^{\text{CH}_2\text{O}}, \quad (\text{S37})$$

where the burial flux of organic matter, $\text{flux}_{\text{bur}}^{\text{CH}_2\text{O}}$, is given by equation (S11). Plugging equations (2), (S11), (S14), (S34), and (S35) into equation (S37) leads us to the following relationship:

$$\text{flux}_{\text{volc}} = \left(\frac{A}{V_p D \alpha} + xy \right) \text{flux}_{\text{marH}_2} + \frac{A}{\alpha} [\text{H}_2] + 2A\alpha \left\{ (1-xy) \frac{\text{flux}_{\text{marH}_2}}{4} \right\}^b.$$

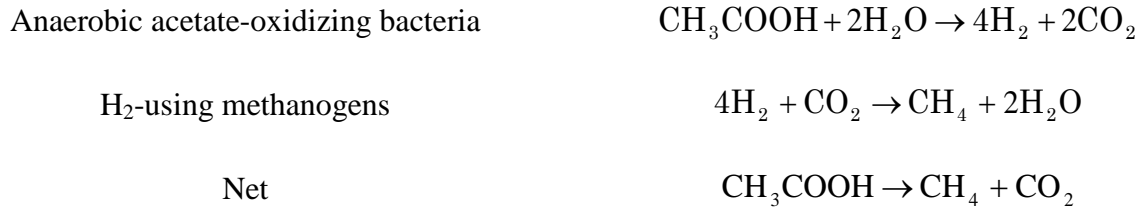
When we take into account photoferrotrophs and Fe(III) reducers, above relationship is modified as follows:

$$\text{flux}_{\text{volc}} = \left(\frac{A}{V_p D \alpha} + xy \right) \text{flux}_{\text{marH}_2} + \frac{A}{\alpha} [\text{H}_2] + 2A\alpha \left\{ (1-xy) \frac{\text{flux}_{\text{marH}_2}}{4} + \frac{1-x-\gamma}{8} \text{flux}_{\text{iron}} \right\}^b - \frac{1-x-\gamma}{2} \text{flux}_{\text{iron}}.$$

These equations can be solved with respect to $\text{flux}_{\text{marH}_2}$ with a numerical scheme. Representative results are shown in Supplementary Fig. 11 (black and red dashed lines). Results demonstrate the basically similar behaviour to that of our Case 1 and 2 biospheres: Because of the low growth

yield of methanogens, higher atmospheric CH₄ levels are required to achieve global redox balance than in anoxygenic photosynthetic biospheres, but the difference of surface temperature between those biospheres does not exceed 2 K.

The alternative biosphere in which acetoclastic methanogens do not exist. As mentioned above, it remains unclear whether acetoclastic methanogens existed in the Archaean anoxic oceans. However, even if acetoclastic methanogens did not exist in Archaean oceans, we can invoke alternative pathways for methane generation; for example, a symbiotic system between anaerobic oxidation of acetate and H₂-based methanogens:



The net stoichiometry is identical to that of acetoclastic methanogens (equation (S9)). In this case, H₂-using methanogens plays a critical role in the methane generation. Here we explore the impact of this alternative biosphere on the biogenic CH₄ cycling. In this system, H₂-based anoxygenic phototrophs are considered as a primary producer, and a fraction of organic matter produced are fermented to acetate, which is converted to CH₄ (and CO₂) by the symbiotic system described above. A part of organic matter produced by H₂-using methanogens (assuming growth yield $y = 0.1$), z , is buried in sediments, and a remaining fraction is fermented to acetate.

The net primary production of H₂-based anoxygenic phototrophs, $NPP_{\text{H}_2\text{-photo}}$, is given by $\text{flux}_{\text{marH}_2}/2$. The production of organic matter by H₂-using methanogens, $NPP_{\text{H}_2\text{-methanogen}}$, is given

by $2 \times y \times \text{flux}_{\text{CH}_3\text{COOH}}$, where $\text{flux}_{\text{CH}_3\text{COOH}}$ represents the production rate of acetate, which is given by:

$$\text{flux}_{\text{CH}_3\text{COOH}} = \frac{1-x}{2} NPP_{\text{H}_2\text{-photo}} + \frac{1-z}{2} NPP_{\text{H}_2\text{-methanogen}} . \quad (\text{S38})$$

Because overall CH_4 generation is given by $(1-y) \times \text{flux}_{\text{CH}_3\text{COOH}}$, solving equation (S38) with respect to $\text{flux}_{\text{CH}_3\text{COOH}}$ gives rise to the following relationship:

$$\text{flux}_{\text{methane}} = \frac{1}{4} \frac{(1-x)(1-y)}{1-(1-z)y} \text{flux}_{\text{marH}_2} . \quad (\text{S39})$$

The burial rate of organic matter is then given by:

$$\text{flux}_{\text{bur}}^{\text{CH}_2\text{O}} = x NPP_{\text{H}_2\text{photo}} + z NPP_{\text{H}_2\text{-methanogen}} . \quad (\text{S40})$$

By adopting the global redox budget equation (S37), the following relationship can be obtained:

$$\text{flux}_{\text{volc}} = \left(\frac{A}{V_p D \alpha} + \frac{x+y(z-x)}{1-(1-z)y} \right) \text{flux}_{\text{marH}_2} + 2A \alpha \left\{ \frac{(1-x)(1-y)}{1-(1-z)y} \frac{\text{flux}_{\text{marH}_2}}{4} \right\}^b .$$

This equation can be solved with respect to $\text{flux}_{\text{marH}_2}$ using a numerical scheme.

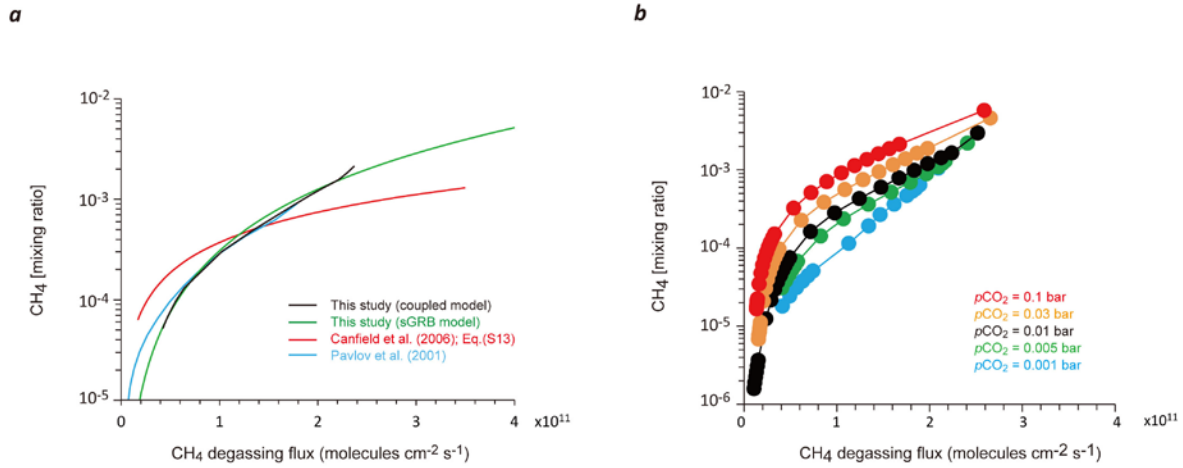
Supplementary Fig. 12 shows representative results. It is clear that if the burial efficiency of organic matter produced by H_2 -using methanogens, z , is equal to x (2%), adopting a symbiotic system as an alternative pathway of biogenic CH_4 generation has a very small effect (<0.3 K) on the model outputs. The maximum effect can be seen when we assume $z = 100\%$ (dashed line). In this extreme case, surface temperature is decreased by <5 K for a given total H_2 outgassing flux.

Supplementary References

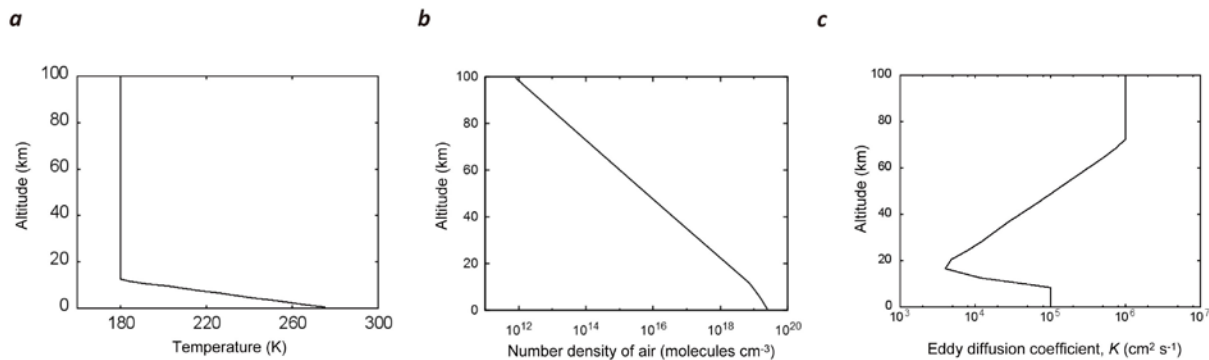
1. Canfield, D. E., Rosing, M. T. & Bjerrum, C. Early anaerobic metabolisms. *Phil. Trans. R. Soc. B* **361**, 1819-1836 (2006).
2. Kharecha, P., Kasting, J. & Siefert, J. A coupled atmosphere–ecosystem model of the early Archean Earth. *Geobiology* **3**, 53-76 (2005).
3. Lyons, T. W., Reinhard, C. T. & Planavsky, N. J. The rise of oxygen in Earth's early ocean and atmosphere. *Nature* **506**, 307-315 (2014).
4. Reinhard, C. T., Raiswell, R., Scott, C., Anbar, A. D. & Lyons, T. W. A Late Archean Sulfidic Sea Stimulated by Early Oxidative Weathering of the Continents. *Science* **326**, 713-716 (2009).
5. Kendall, B., Anbar, A. D., Kappler, A. & Konhauser, K. O. The Global Iron Cycle. In: Knoll A. H., Canfield, D. E. & Konhauser, K. O. (eds). *Fundamentals of Geobiology*. (John Wiley & Sons, Ltd: Oxford, 2012).
6. Halevy, I., Alesker, M., Schuster, E. M., Popovitz-Biro, R. & Feldman, Y. A key role for green rust in the Precambrian oceans and the genesis of iron formations. *Nat. Geosci.* **10**, 135-139 (2017).
7. Konhauser, K. O., Newman, D. K. & Kappler, A. The potential significance of microbial Fe(III) reduction during deposition of Precambrian banded iron formations. *Geobiology* **3**, 167-177 (2005).
8. Rothman, D. H., *et al.* Methanogenic burst in the end-Permian carbon cycle. *Proc. Natl Acad. Sci. USA* **111**, 5462-5467 (2014).
9. Crowe, S. A., *et al.* Sulfate was a trace constituent of Archean seawater. *Science* **346**, 735-739 (2014).
10. Zhelezinskaia, I., Kaufman, A. J., Farquhar, J. & Cliff, J. Large sulfur isotope fractionations associated with Neoproterozoic microbial sulfate reduction. *Science* **346**, 742-744 (2014).

11. Beal, E. J., House, C. H. & Orphan, V. J. Manganese- and Iron-Dependent Marine Methane Oxidation. *Science* **325**, 184-187 (2009).
12. Pavlov, A. A., Brown, L. L. & Kasting, J. F. UV shielding of NH₃ and O₂ by organic hazes in the Archean atmosphere. *J. Geophys. Res.* **106**, 23267-23287 (2001).
13. Walker, J. C. G. *Evolution of the atmosphere*. (Macmillan, New York, 1977).
14. Kasting, J. F. What caused the rise of atmospheric O₂? *Chem. Geol.* **362**, 13-25 (2013).
15. Massie, S. T. & Hunten, D. M. Stratospheric eddy diffusion coefficients from tracer data. *J. Geophys. Res.* **86**, 9859-9868 (1981).
16. Catling, D. C. & Kasting, J. F. *Atmospheric Evolution on Inhabited and Lifeless Worlds*. (Cambridge University Press, Cambridge, 2017).
17. Battistuzzi, F. U., Feijao, A. & Hedges, S. B. A genomic timescale of prokaryote evolution: insights into the origin of methanogenesis, phototrophy, and the colonization of land. *BMC Evol. Biol.* **4**, 44-44 (2004).
18. Moore, E. K., Jelen, B. I., Giovannelli, D., Raanan, H. & Falkowski, P. G. Metal availability and the expanding network of microbial metabolisms in the Archaean eon. *Nat. Geosci.* **10**, 629-636 (2017).
19. Ueno, Y., Yamada, K., Yoshida, N., Maruyama, S. & Isozaki, Y. Evidence from fluid inclusions for microbial methanogenesis in the early Archaean era. *Nature* **440**, 516-519 (2006).

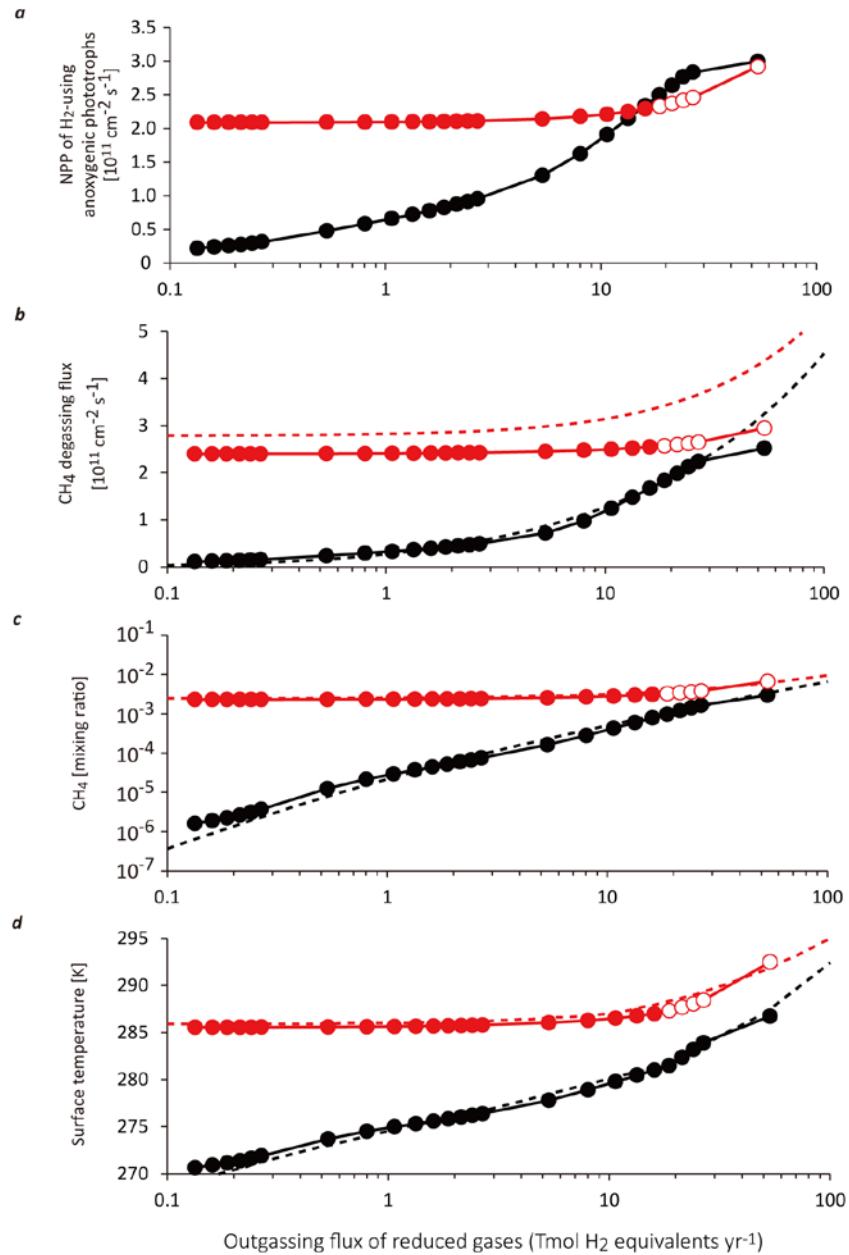
Supplementary figures:



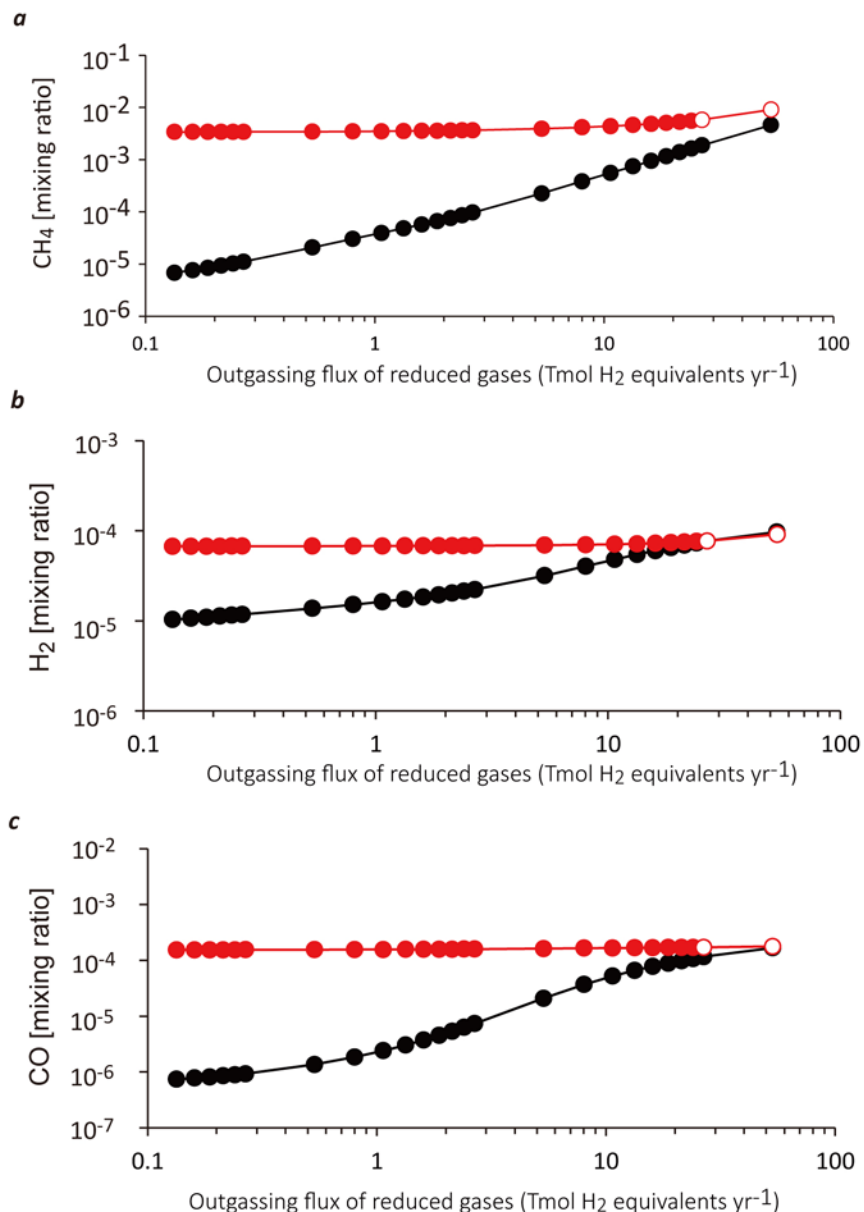
Supplementary Fig. 1. Empirical relationship between atmospheric CH₄ mixing ratio and CH₄ degassing flux from the ocean to the atmosphere. (a) Photochemical model solutions with assuming atmospheric CO₂ level of 0.01 bar is shown as a black line, which is compared with the results presented in Pavlov et al.¹² (blue line). The green curve denotes the fitting solution for our photochemical model results (equation (2) in Methods). The previously proposed linear solution¹ is also shown as a red line. (b) Atmospheric $f(\text{CH}_4)$ as a function of CH₄ degassing flux from the ocean for different assumed values of the atmospheric $p\text{CO}_2$.



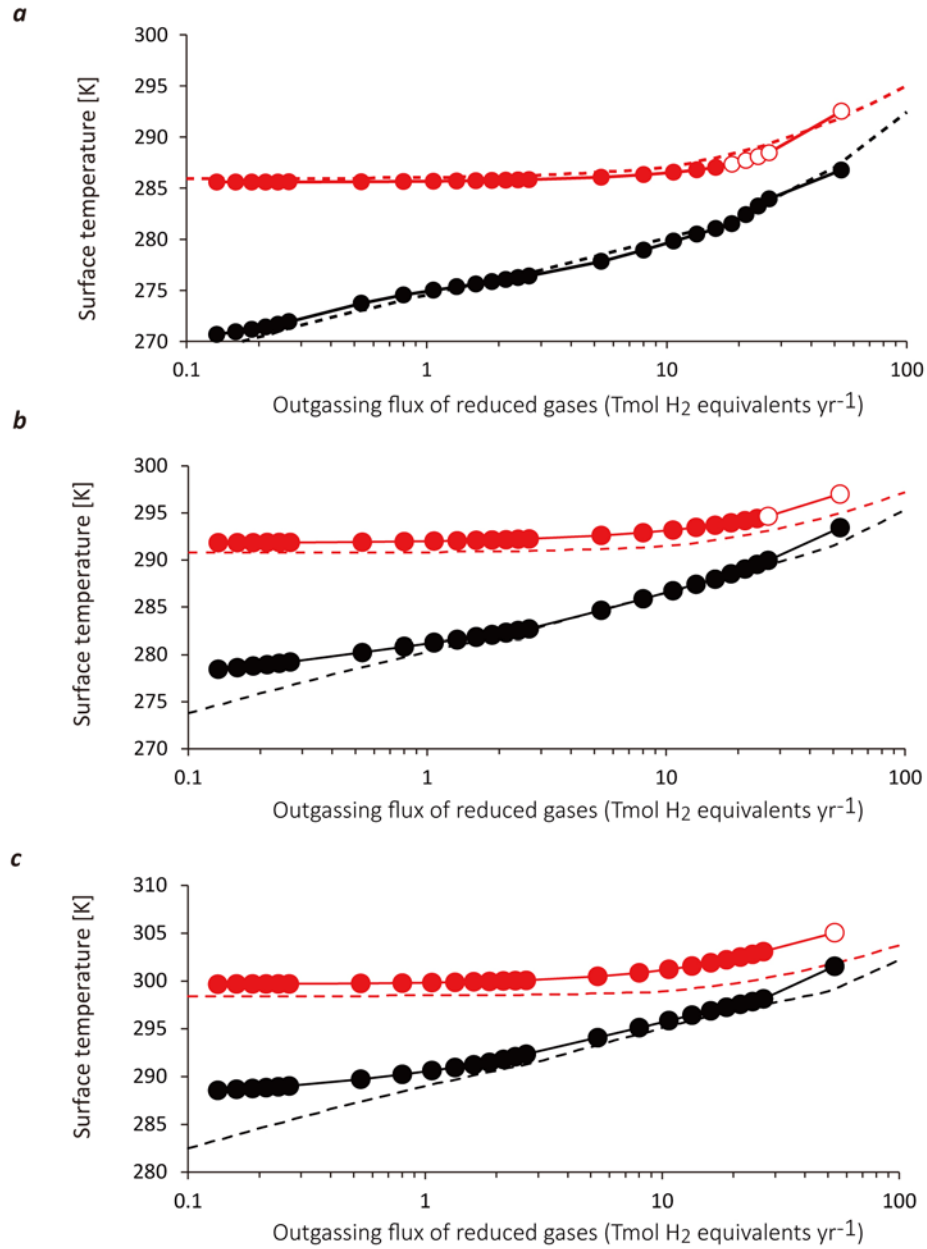
Supplementary Fig. 2. The profiles assumed in the photochemical model. (a) temperature, (b) number density of air, and (c) eddy diffusion coefficient¹⁵ used in the photochemical model.



Supplementary Fig. 3. The biogeochemical response to changes in the outgassing flux of reduced species. The values of model parameters are equal to that of Fig. 2 in the main text (i.e., $x = 0.02$, $\text{flux}_{\text{iron}} = 80 \text{ Tmol yr}^{-1}$, and $\gamma = 0$), except for atmospheric $p\text{CO}_2$ ($= 33 \text{ PAL}$). **(a)** NPP of H₂-using anoxygenic photosynthesis. **(b)** Biogenic CH₄ degassing flux from the ocean to the atmosphere. **(c)** Mixing ratio of CH₄ in the atmosphere. **(d)** Global surface temperature. Solid lines with circles show results obtained with a coupled atmosphere-ecosystem model, and dashed lines in **(b)**, **(c)** and **(d)** represent solutions obtained by the sGRB model. Black and red lines represent results for the Case 1 and Case 2 biosphere, respectively. Unfilled circles indicate unconverged solutions (see Methods). Note a logarithmic scale in y-axis of **(c)**.

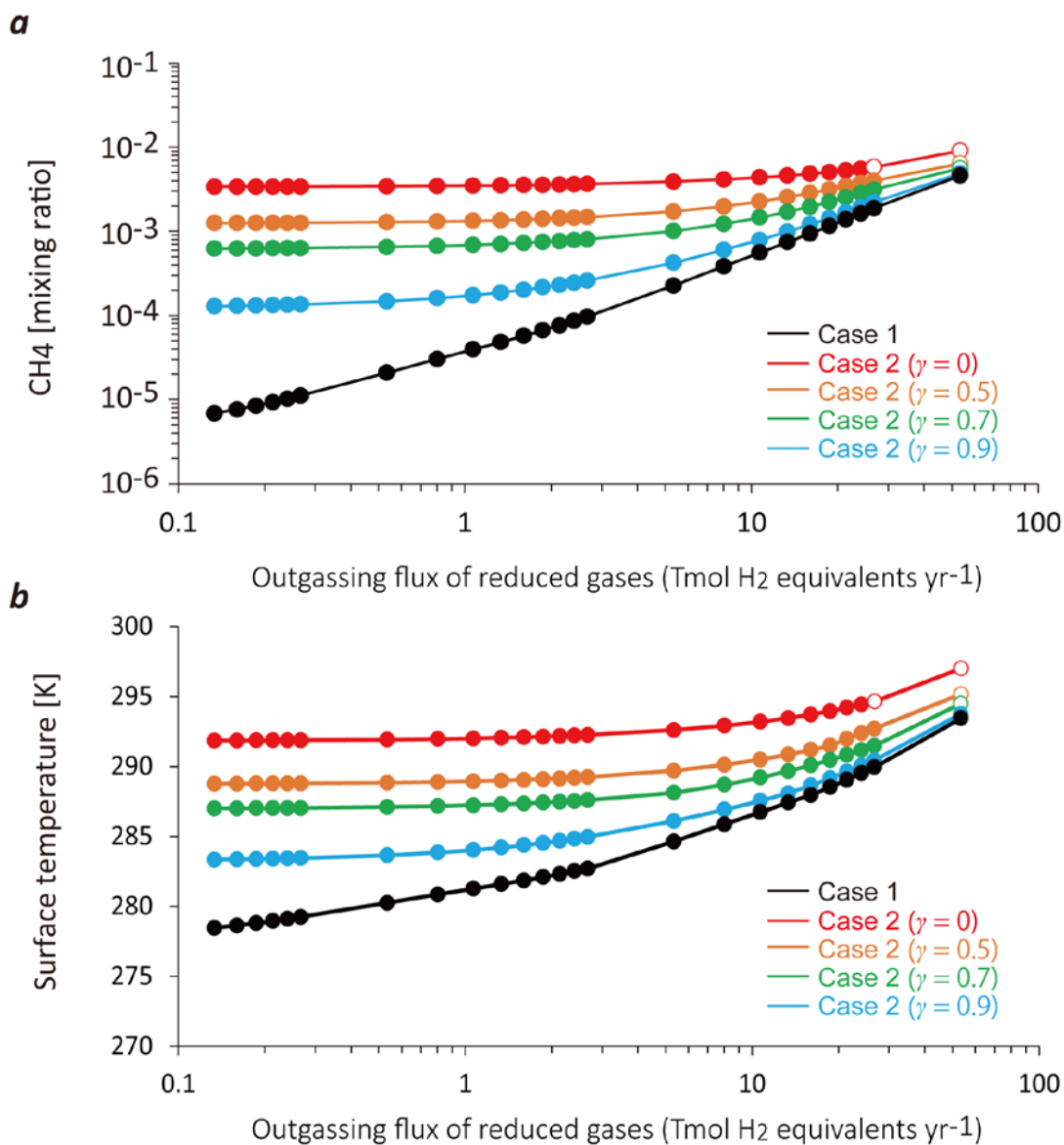


Supplementary Fig. 4. Photochemical model results showing the response of atmospheric composition to changes in H₂ volcanic degassing flux. Parameter values are identical to those for Fig. 2 of the main text. Mixing ratios of CH₄ (a), H₂ (b), and CO (c). Black lines with circles represent the results for the Case 1 biosphere (H₂-based ecosystem). Red lines with circles represent the results for the Case 2 biosphere (hybrid H₂/Fe²⁺ ecosystem). Unfilled circles indicate unconverged solutions.

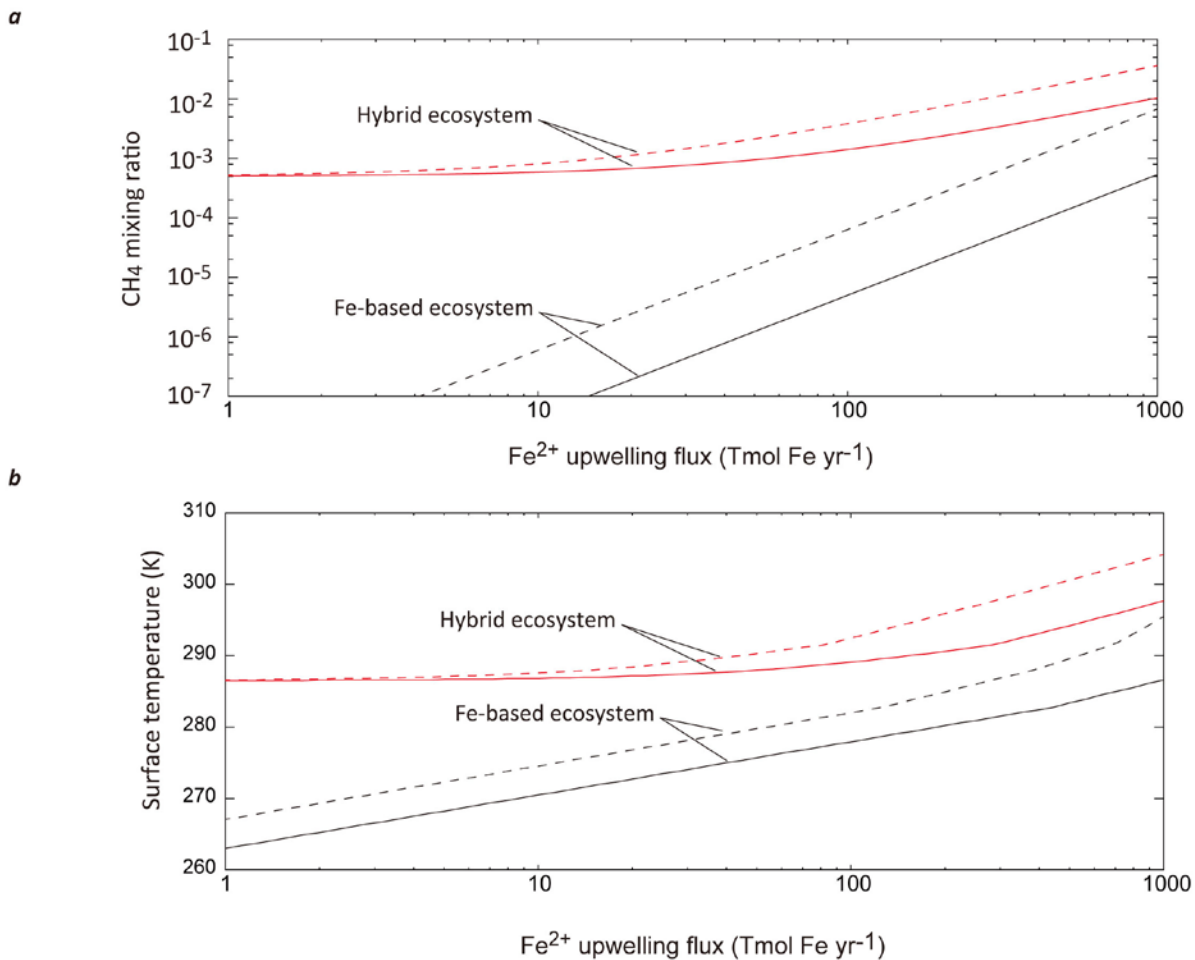


Supplementary Fig. 5. Model comparison between the coupled model and sGRB model.

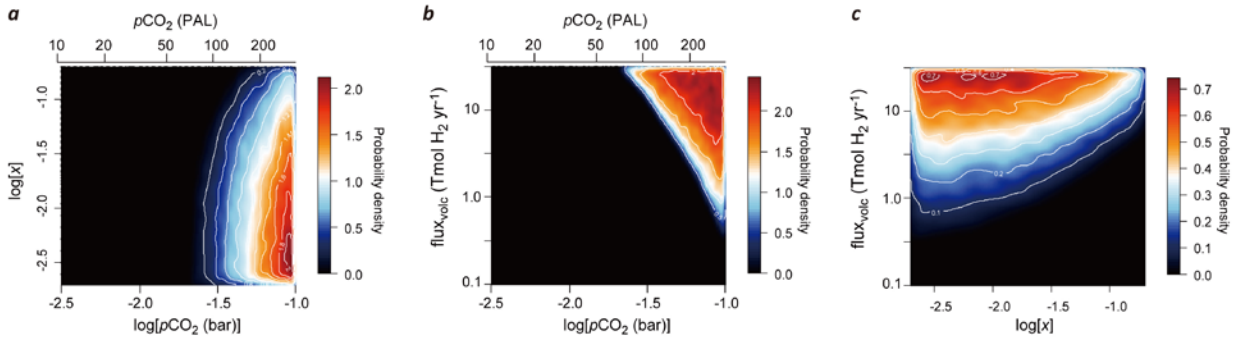
The global average surface temperature as a function of total H₂ outgassing flux with different values of atmospheric $p\text{CO}_2$: **(a)** 33 PAL (0.01 bar), **(b)** 100 PAL (0.03 bar), and **(c)** 330 PAL (~0.1bar). Solid lines with circles denote results obtained with a coupled model. The dashed lines are solutions obtained by the sGRB model. Black and red colours represent the Case 1 and Case 2 results, respectively. Unfilled circles indicate unconverged solutions. Note a different scale in y-axis of **(c)**. The values of model parameters are equal to that of Fig. 2 in the main text (i.e., $x = 0.02$, $\text{flux}_{\text{iron}} = 80 \text{ Tmol yr}^{-1}$, and $\gamma = 0$).



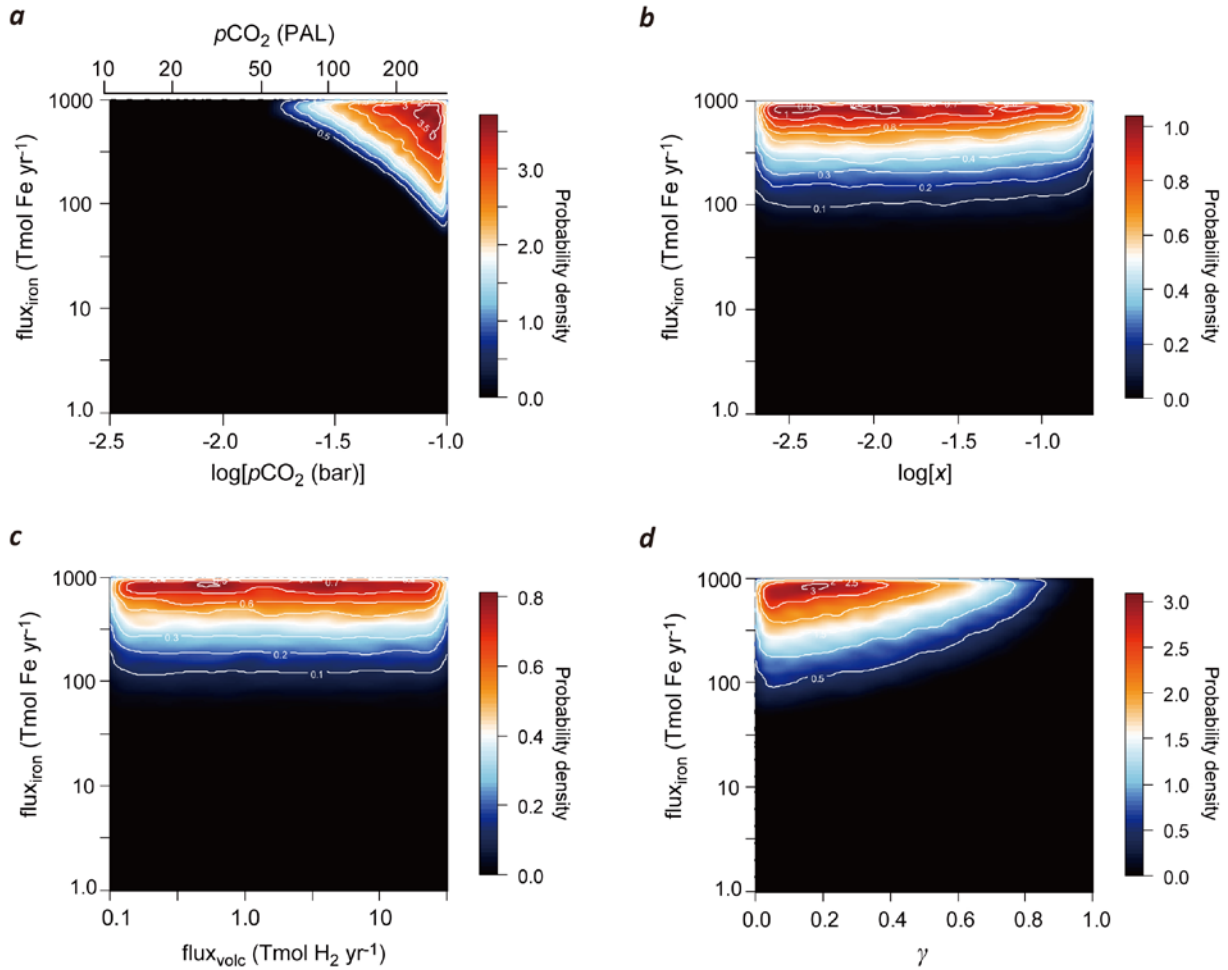
Supplementary Fig. 6. The coupled atmosphere-ocean ecosystem model results showing the effect of γ . The values of model parameters are equal to that of Fig. 2 in the main text (i.e., $x = 0.02$, $\text{flux}_{\text{iron}} = 80 \text{ Tmol yr}^{-1}$, and $p\text{CO}_2 = 100\text{PAL}$). The response of (a) atmospheric CH₄ mixing ratio and (b) global surface temperature to changes in outgassing flux of reductants ($\text{flux}_{\text{volc}}$) with different values of γ .



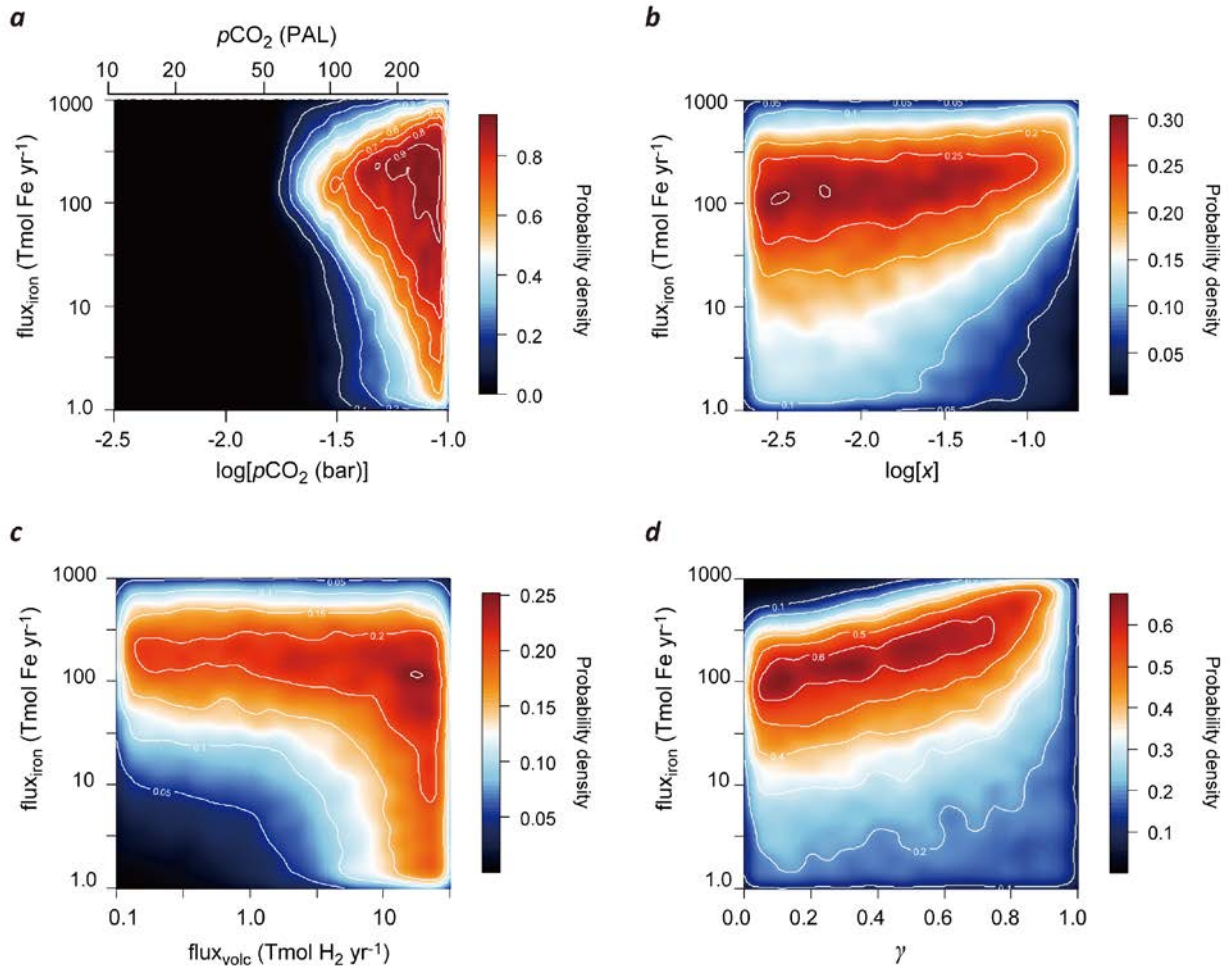
Supplementary Fig. 7. The sGRB model result on the effect of the Fe²⁺ flux. The Fe²⁺ input flux is varied from 1 to 1000 Tmol Fe yr⁻¹ while holding total H₂ outgassing rate at 10 Tmol yr⁻¹. The response of (a) atmospheric mixing ratio of CH₄ and (b) surface temperature to changes in Fe²⁺ upwelling flux to the ocean surface, with different values of γ (0 = dashed lines; 0.7 = solid lines). Black lines denote results from the Fe-based ecosystem, in which H₂-based anoxygenic phototrophs are removed from the Case 2 hybrid ecosystem. Red lines represent results for the Case 2 hybrid ecosystem. The values of atmospheric $p\text{CO}_2$ and x are equal to that of Fig. 2 in the main text (i.e., $p\text{CO}_2 = 100 \text{ PAL}$ and $x = 0.02$).



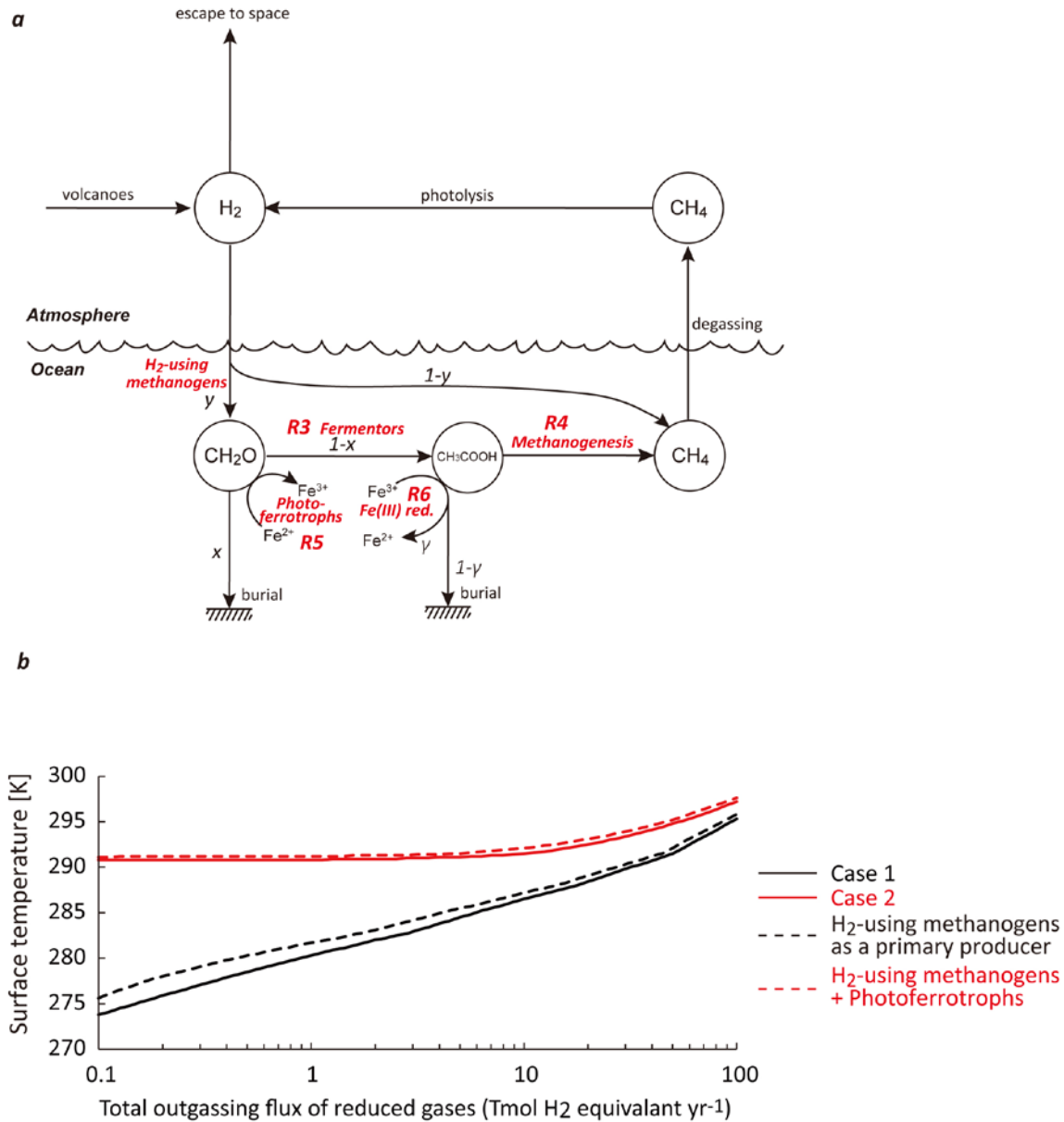
Supplementary Fig. 8. Monte Carlo simulations showing the probability density for warm (≥ 288 K) climate states for the Case 1 biosphere. (a) $\log(x)$ – $\log(p\text{CO}_2)$ phase space, (b) $\text{flux}_{\text{volc}}$ – $\log(p\text{CO}_2)$ phase space, and (c) $\text{flux}_{\text{volc}}$ – $\log(x)$ phase space. Black areas indicate parameter space where no warm solutions exist. Warm colours (orange and red) represent higher probability than cold colours (blue and white).



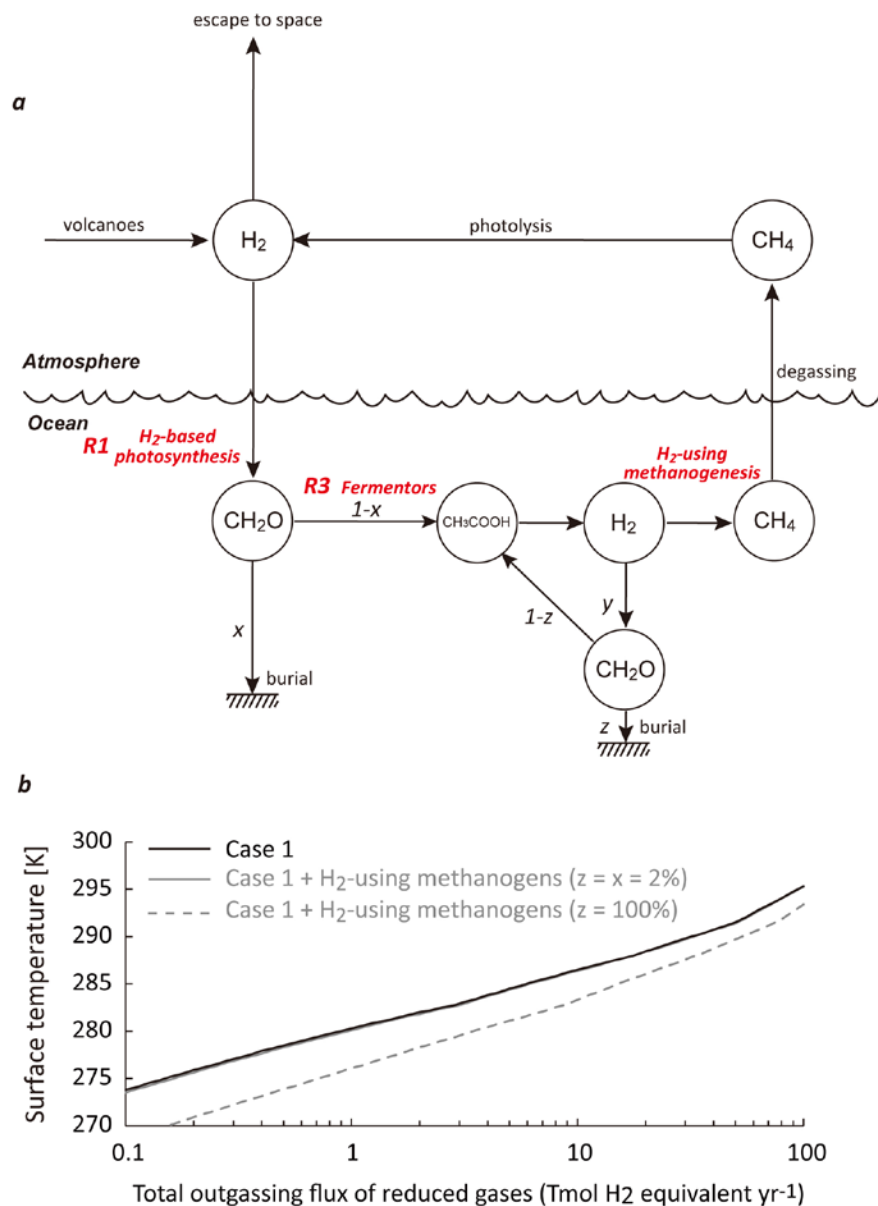
Supplementary Fig. 9. Monte Carlo simulations showing the probability density for warm (≥ 288 K) climate states for the Fe-based biosphere. The H_2 -based anoxygenic phototrophs are removed from the Case 2 biosphere. (a) $flux_{iron}$ – $\log(pCO_2)$ phase space, (b) $flux_{iron}$ – $\log(x)$ phase space, (c) $flux_{iron}$ – $flux_{volc}$ phase space, and (d) $flux_{iron}$ – γ phase space. Black areas indicate parameter space where no warm solutions exist. Warm colours (orange and red) represent higher probability than cold colours (blue and white).



Supplementary Fig. 10. Monte Carlo simulations showing the probability density for warm (≥ 288 K) climate states for the Case 2 hybrid biosphere. (a) $\text{flux}_{\text{iron}}-\log(p\text{CO}_2)$ phase space, (b) $\text{flux}_{\text{iron}}-\log(x)$ phase space, (c) $\text{flux}_{\text{iron}}-\text{flux}_{\text{volc}}$ phase space, and (d) $\text{flux}_{\text{iron}}-\gamma$ phase space. Black areas indicate parameter space where no warm solutions exist. Warm colours (orange and red) represent higher probability than cold colours (blue and white).



Supplementary Fig. 11. sGRB model results for the biosphere in which H₂-using methanogens are considered as a primary producer. (a) Schematic diagram of the biosphere considered here. Organic matter is produced by H₂-using methanogens (assuming a growth yield, y , of 0.1 (ref.^{1,2})) and photoferrotrophs (R5). A fraction of organic matter produced, x , is buried in sediments and the remaining fraction is decomposed to CH₄ (and CO₂). **(b)** Surface temperature response to changes in the total outgassing flux of reduced gases. Solid black and red lines denote solutions for our Case 1 and 2 biospheres, respectively. Dashed lines represent results for biospheres considered here (red line = without photoferrotrophs; black line = with photoferrotrophs). The values of model parameters are equal to that of Fig. 2 in the main text (i.e., $x = 2\%$, $p\text{CO}_2 = 100$ PAL, $\text{flux}_{\text{iron}} = 80$ Tmol Fe yr⁻¹, and $\gamma = 0$).



Supplementary Fig. 12. sGRB model results for the alternative biosphere in which acetic acid is converted to CH_4 via a syntrophic system between anaerobic acetate-oxidation bacteria and H_2 -using methanogens. (a) Schematic diagram of the biosphere considered here. H_2 -based anoxygenic photosynthesis (R1) is considered as a primary producer. A fraction of organic matter produced is fermented to acetate, which is converted to CH_4 by a symbiotic system of acetate-oxidizing bacteria and H_2 -using methanogens. A fraction of organic matter produced by H_2 -using methanogens (assuming growth yield $y = 0.1$), z , is buried in sediments. **(b)** Surface temperature response to changes in the total outgassing flux of reduced gases. The black line denotes solutions for our Case 1 biosphere. Grey lines represent results for the biosphere considered here, with different values of z (2% = solid; 100% = dashed). The values of model parameters are equal to that of Fig. 2 in the main text (i.e., $x = 2\%$ and $pCO_2 = 100$ PAL).

Supplementary Table 1. Metabolisms considered in this study.

Reaction #	Stoichiometry	Case 1	Case 2
R1	$2\text{H}_2 + \text{CO}_2 \rightarrow \text{CH}_2\text{O} + \text{H}_2\text{O}$	•	•
R2	$4\text{CO} + 2\text{H}_2\text{O} \rightarrow 2\text{CO}_2 + \text{CH}_3\text{COOH}$	•	•
R3	$2\text{CH}_2\text{O} \rightarrow \text{CH}_3\text{COOH}$	•	•
R4	$\text{CH}_3\text{COOH} \rightarrow \text{CH}_4 + \text{CO}_2$	•	•
R5	$4\text{Fe}^{2+} + 11\text{H}_2\text{O} + \text{CO}_2 \rightarrow 4\text{Fe}(\text{OH})_3 + \text{CH}_2\text{O} + 8\text{H}^+$		•
R6	$\text{CH}_3\text{COOH} + 8\text{Fe}(\text{OH})_3 + 16\text{H}^+ \rightarrow 8\text{Fe}^{2+} + 2\text{CO}_2 + 22\text{H}_2\text{O}$		•

Supplementary Table 2. Example of chemical species considered in this study and its reducing power in units scaled to the reducing power of H₂ that is defined as +1 (ref.^{14, 16}).

Species	Reducing power
H ₂ O	0
CO ₂	0
N ₂	0
FeO	0
SO ₂	0
H ₂	+1
O ₂	-2
CH ₄	+4
CH ₂ O	+2
CO	+1
NH ₃	+1.5
NO	-1
NO ₂	-2
HNO ₃	-2.5
Fe(OH) ₃	-0.5
S ₂	+4
H ₂ S	+3
H ₂ SO ₄	-1

Supplementary Table 3. Chemical species included in the 1-D photochemical model

Long-lived species	O, O ₂ , H ₂ O, H, OH, HO ₂ , H ₂ O ₂ , H ₂ , CO, HCO, H ₂ CO, CH ₄ , CH ₃ , C ₂ H ₆ , NO, NO ₂ , HNO, H ₂ S, HS, S, SO, SO ₂ , H ₂ SO ₄ , HSO, S ₂ , NH ₃ , NH ₂ , N ₂ H ₃ , N ₂ H ₄ , ³ CH ₂ , C ₂ H ₅ , C ₂ H ₂ , C ₂ H ₄ , C ₃ H ₈ , C ₂ H ₃ , C ₃ H ₆ , C ₃ H ₂ , CH ₂ C ₂ H ₂ , CH ₃ C ₂ H
Short-lived species	HNO ₂ , HNO ₃ , NH, N, O ₃ , O(¹ D), ¹ SO ₂ , ³ SO ₂ , HSO ₃ , SO ₃ , S ₃ , S ₄ , NH ₂ X, C ₂ , C ₂ H, C ₃ H ₇ , C ₃ H ₃ , CH, C, C ₃ H ₅ , C ₂ H ₄ OH, CH ₃ CHO, CH ₃ CO, C ₂ H ₂ OH, CH ₂ CO, ¹ CH ₂ , CH ₃ O, C ₂ H ₅ CHO
Aerosol particles	elemental sulphur-aerosol, sulfate-aerosol, hydrocarbon-aerosol
Relatively inert species	N ₂ , CO ₂

Supplementary Table 4. Comparison of different biospheres of Monte Carlo simulations.

Biosphere	Criteria for adoption	Total sampling #	# TRUE	# FALSE	Adoption rate (%)
Case 1	$T \geq 288 \text{ K}, \text{CH}_4/\text{CO}_2 \leq 0.2$	855,232	100,000	755,232	11.7
Fe-based*	$T \geq 288 \text{ K}, \text{CH}_4/\text{CO}_2 \leq 0.2$	1,830,767	100,000	1,730,767	5.46
Case 2	$T \geq 288 \text{ K}, \text{CH}_4/\text{CO}_2 \leq 0.2$	423,430	100,000	323,430	23.6

*Fig. 3c of the main text.